Supporting Information

Photo-modulation of the work function and electronic properties of MXenes *via* a self-assembled cationic azobenzene molecular layer

Yan Fang[a], Tian Wang[a], Jiahui Xu[a], Jingyi Xiao[b], Yin-Shan Meng[a,c]* and Tao Liu[a,c]*

[a]*State Key Laboratory of Fine Chemicals, Frontier Science Center for Smart Materials, School of Chemical Engineering, Dalian University of Technology, 2 Linggong Road, Dalian 116024, China. Corresponding authors: mengys@dlut.edu.cn, liutao@dlut.edu.cn*

[b]*Instrumental Analysis Center, Dalian University of Technology, No.2 Linggong Rd., 116024 Dalian, China*

[c]*Liaoning Binhai Laboratory, Dalian, 116023, China., P. R. China.*

Contents

Section S1: materials and methods

Section S2: supplementary Scheme S1–S2, Fig. S1–S7, and Table S1–S7

Section S1: materials and methods

Titanium Aluminum Carbide (Ti_3AlC_2, 200 mesh) was purchased from Jilin 11 Technology Co., Ltd. Hydrochloric acid (HCl), lithium fluoride (LiF), and 3-aminopropyltriethoxysilane (APTES) was obtained from Shanghai Maclean Biochemical Technology Co., Ltd. All chemicals and reagents were of analytical purity and used without any further purification. Deionized water (DI water) was used in all experiments. For the light-switching experiments, a laser diode pumped Nd:YAG lasers (λ = 365 nm, 0.2 mW; λ = 473 nm, 1.0 mW) was used as UV light and visible light source, respectively. Powder X-ray diffraction (PXRD) patterns were recorded on a Bruker D8 Advanced X-ray Diffractometer (Cu-Kα radiation: λ = 1.5406 Å). Transmission electron microscopy (TEM) was taken on a JEM-F200 microscope operating at 200 kV. Atomic force microscopy (AFM) measurements were performed in a non-contact mode with a Bruker JPK NanoWizard 4XP, AFM images were processed using AIST-NT imaging analysis and processing software (Version 3.2.14). The samples were drop-casted onto freshly cleaved mica substrates. Element mapping was characterized using a field emission scanning electron microscope (FE-SEM, SU8220) with an acceleration voltage of 15.0 kV. X-ray photoelectron spectroscopy (XPS) measurements were conducted on Thermo Scientific K-Alpha+ spectrometer. All binding energies were calibrated by referencing C 1s peak at 284.8 eV. UV–vis transmission and absorption spectra were recorded from 200 to 1000 nm using a UH4150 spectrometer with a bare quartz cover plate as the baseline. Raman spectra were recorded on a Renishaw InVia spectrometer using a 785 nm excitation laser. The excitation power was kept at 0.1 mW to avoid local heating. The scattered light was collected with a 100× objective lens. Optical images of the films were acquired using a conventional optical microscope. Hall effect measurements were performed at room temperature using the van der Pauw configuration (Lake Shore Cryotronics, Ltd.), with the device active area measured to be approximately 1.0 × 1.0 cm^2.

Water contact angle (CA) measurement

Static water contact angles were measured using an SDC-350 goniometer (Pue Instrument Technology Co., Ltd) with deionized water droplets (3 μL) dispensed at a rate of 3 μL/s. The captured images were analyzed using ImageJ software.

Kelvin probe microscopy (KPFM)

KPFM measurements were performed on a Bruker Dimension FastScan employing a Pt-Ir coated Si cantilever with a drive frequency of 67 kHz. All measurements were operated in non-contact mode under ambient conditions. The average work function was recorded in the area of 5 × 5 μm^2, with potential maps collected simultaneously with the topography. Highly oriented pyrolytic graphite (HOPG) was used as a reference to convert the measured contact potential difference (V_{CPD}) into the actual work function values. Data processing was conducted using NanoScope Analysis software. The processing procedure is as follows: (i) Multi-line scanning: Draw multiple scan lines (n > 6) across the target domains. (ii) Numerical extraction: Export the potential value of each scan line and integrate them into a dataset (n > 150). (iii) Statistical calculation: Calculate the arithmetic mean and standard deviation of the dataset. Photo-induced isomerization experiments were carried out in an *ex situ* manner.

Conductance measurement

Conductance variations of the device were recorded on the CHI660E electrochemical workstation (Shanghai Chenhua, China) with a fixed voltage of 0.5 V throughout all experiments. The AZ^+-$Ti_3C_2T_x$ device was placed inside a home-made chamber, with Cu wire connected to internally mounted alligator clips. The chamber was sealed to prevent external air ingress. Real-time resistance was measured using electrochemical analyzers in a two-electrode configuration. Prior to testing, the chamber was purged with dry N_2 gas to

establish a stable baseline resistance, after which the device was exposed to light irradiation for measurement. The data were from multiple devices (n > 3) and repeatable over five irradiation cycles. The photocurrent switching amplitude is calculated as follows: $(I - I_0) / I_0 * 100$, where I_0 and I represent the current value before and after irradiation, respectively.

Synthesis of $Ti_3C_2T_X$ MXene nanosheets

$Ti_3C_2T_x$ nanosheets were synthesized by selectively etching the Al layers from Ti_3AlC_2 (MAX) using the method previously reported.[1] Briefly, 1 g of LiF was added to 20 mL of 9 mol L^{-1} HCl and stirred with a Teflon magnetic stir bar. Then, 1 g of Ti_3AlC_2 was slowly added into the LiF/HCl etchant solution and allowed to react for 24 h at 40 °C. The resulting dark grey resultant was washed with deionized water and decanted repeatedly to remove the acidic supernatant until the pH reached approximately 6.0. The neutral suspension was then sonicated in an ice-water bath for 30 min under argon protection to delaminate the $Ti_3C_2T_x$ flakes. Finally, the dark green solution was centrifuged at 3500 rpm for 30 min, and the upper black supernatant was collected for the fabrication of $Ti_3C_2T_x$ monolayer via an interfacial self-assembly deposition technique.

Fabrication of MXene monolayers

The obtained $Ti_3C_2T_x$ colloidal solution was deposited on SiO_2/Si substrates using an interfacial self-assembly method. Briefly, the substrates were pre-treated with 10% NaOH solution for 24 h, rinsed with DI water, and dried under a N_2 stream. APTES was prepared in ethanol (vol ratio, 1 : 50). The substrates were immersed in APTES solution for 24 h at room temperature. The functionalized substrates were then rinsed with DI water to remove excess APTES and blown dry with N_2 stream. To form self-assembled monolayers, the pre-treated substrates were immersed in a 10% MXene colloidal solution, thoroughly rinsed with DI water, and dried in a vacuum oven. This process was repeated until an optimal MXene film was obtained.

Synthesis of AZ^+Br^- cationic derivatives

Cationic azobenzene-containing moieties, butylazobenzene dimethylammonium bromide, AZ^+Br^-, was prepared according to the previous literature.[2]

Fabrication of AZ^+-$Ti_3C_2T_x$ device

Briefly, AZ^+Br^- solutions with different concentrations (0, 0.5, 1.0, 1.5 and 2.0 mM) were prepared in DI water. The self-assembled MXene substrates were subsequently immersed in the above AZ^+Br^- solutions, and incubated at 37 °C for 10 min, followed by rinsing with DI water to remove extra AZ^+ species. Finally, the resulting AZ^+-$Ti_3C_2T_x$ devices were dried under a N_2 stream, and stored in glass dishes prior for measurements.

Section S2: supplementary Scheme S1–S2, Fig. S1–S7, and Table S1–S7

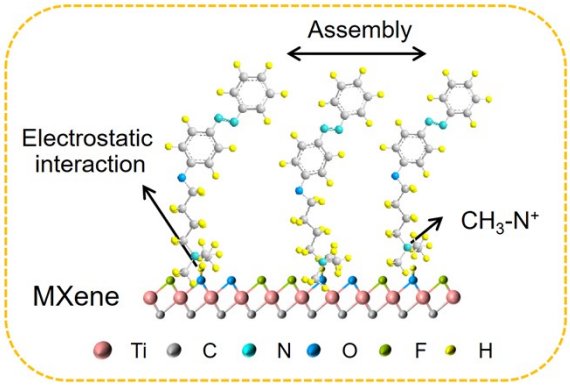

Scheme S1 Schematic representation of the self-assembly of AZ^+ moieties on the MXene substrate.

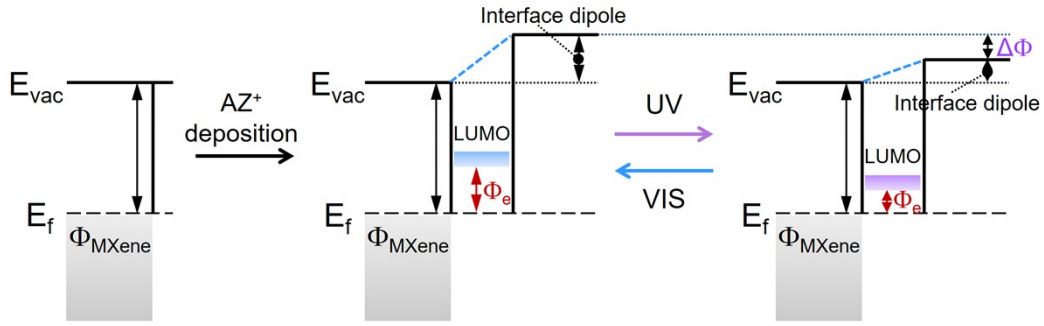

Scheme S2 Schematic illustration of the changes in the WF due to photo-isomerization of AZ^+: (left) schematic energy level diagram for an untreated interface (without AZ^+ deposition); (middle) *trans*-AZ^+ imposes an interface dipole that increases the local vacuum energy level (E_{vac}); (right) photo-isomerization to *cis*-AZ^+ imposes an interface dipole that decreases E_{vac}. Φ_{MXene} is the WF of MXene, and Φ_e denotes the electron injection barrier. $\Delta\Phi$ is the local WF change resulting from the *trans-cis* conformation. The zero energy is set at the Fermi level (E_f) so that the WF can be directly readable.[3,4]

Scanning electron microscopy (SEM) images

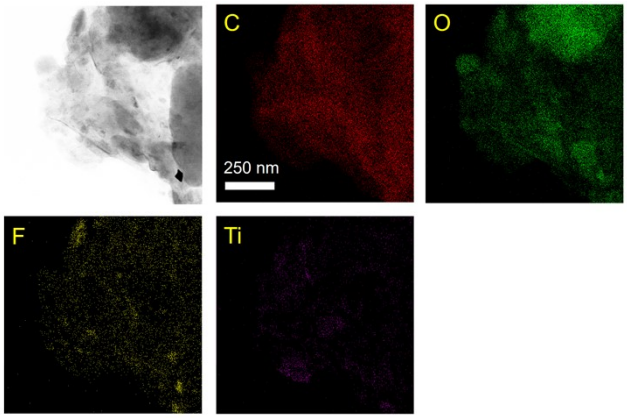

Fig. S1 TEM image of $Ti_3C_2T_x$, and the corresponding energy dispersive X-ray elemental mappings for C, O, F, and Ti.

Atomic force microscopy (AFM) measurement

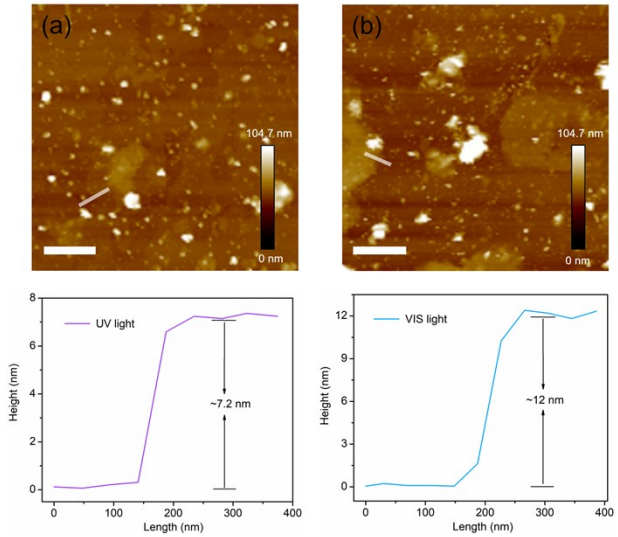

Fig. S2 AFM images (with height profiles) of AZ^{+}-$Ti_3C_2T_x$ film exposure to (a) UV, and (b) VIS light, respectively.

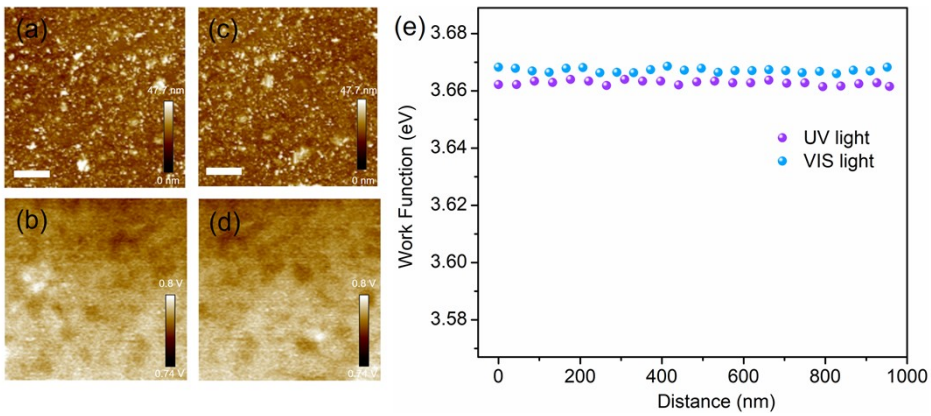

Fig. S3 KPFM images and the corresponding work function of MXene film exposure to (a,b) UV, and (c,d) VIS light, respectively. Scale bar: 1 um. (e) Plot of the converted work function as a function of distance based on the profiles (b) and (d).

Conductance measurement

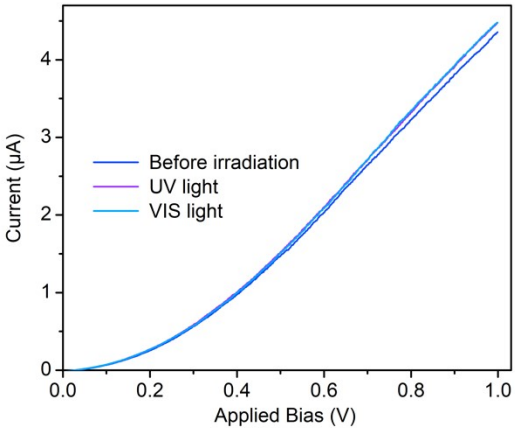

Fig. S4 *I–V* characteristics of bare $Ti_3C_2T_x$ substrate.

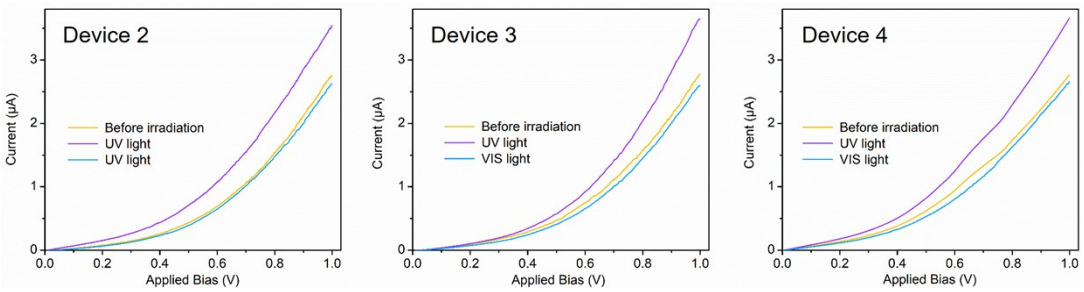

Fig. S5 Single-cycle light irradiation of three AZ^{+}-$Ti_3C_2T_x$ devices.

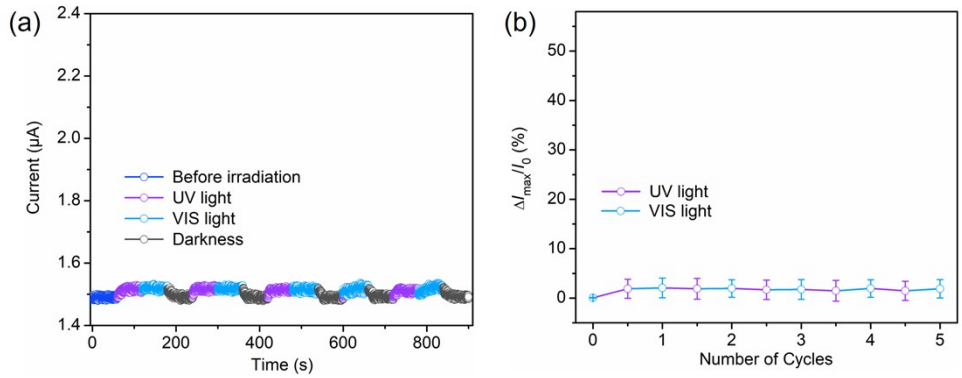

Fig. S6 (a) Photocurrent measurement of $Ti_3C_2T_x$ for 0.5 V applied during UV and VIS irradiation cycles, and (b) Calculation of maximum current switching amplitude.

The CTAB-MXene device was prepared as a non-photoactive cationic control. As shown in Fig. S7, the conductivity of CTAB-MXene exhibited negligible variation under light irradiation, confirming that the reversible regulation of electrical properties originates predominantly from the photo-induced isomerization of AZ^+ molecules rather than from electrostatic doping effects.

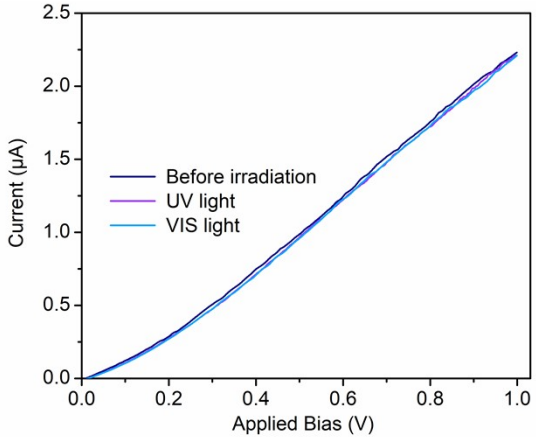

Fig. S7 *I–V* characteristics of CTAB-$Ti_3C_2T_x$ device.

Estimation of the functionalization efficiency of MXene with AZ^+

The functionalization efficiency of AZ^+ attachment to the MXene surface is calculated using the four different N 1s component peaks shown in high-resolution N 1s spectrum. The percent functional efficiency (% AZ^+) is obtained by determining the contribution from the AZ^+ moieties and relating it to the total nitrogen detected within the sample:

Table S1 Calculation of the N 1s component peaks in N 1s spectrum.

Name	Peak BE	% Area
$C–NH_2$	398.4	10.5
N=N	399.8	65.3
$C–NH_3^+$	401.9	14.4
$N–CH_3$	403.6	9.8

To determine the surface coverage of AZ^+, we use Ti–C as the reference signal because it is not subject to by the functionalization and the environment. The area ratios of other component peaks can then be compared to the stoichiometric ratios of Ti–C peak. From each ratio of the measured areas from the sample I_N and the MXene substrate I_{Ti}, the atomic density of ρ_N relative to ρ_{Ti} can be calculated based on the equation:[5]

$$\rho_N = \left(\frac{I_N/S_N}{I_{Ti}/S_{Ti}}\right) \times \rho_{Ti} \qquad (S1)$$

Where I_N is the measured area of AZ^+ moieties; I_{Ti} represents the increased area of Ti–O peaks after functionalization; S_N and S_{Ti} are the sensitivity factors of N and Ti elements, respectively. S_N: 1.67, S_{Ti}: 6.47. Ti density of the MXene film (ρ_{Ti} = 3.7 * 10^{18} atoms cm^{-2}) is used in the calculation.

Each AZ^+ moiety contributes three N atoms. The number of molecular concentration per unit area of Ti atom is determined:

$$\sigma_{Az} = \frac{\rho_N}{3} \qquad (S2)$$

Table S2 Calculation of the peak areas in XPS spectrum.

Area / Sample	Ti–C	Ti–O	C–N	N=N/N–C
MXene	82511.2	58583.9	11800.8	—
AZ^+-$Ti_3C_2T_x$	15039.1	26619.3	1930.7	5819.1

Note: the area is obtained by integrating the respective peaks, and the unit is CPS.eV.

Contact angle measurement

Table S3 Calculation of CA of the sample.

Sample		λ / nm	CA / °
MXene	0	—	51.7 ± 0.45°
AZ^+-$Ti_3C_2T_x$	0	—	70.7 ± 0.3
	0.5	365	63.8 ± 0.21
	1.0	473	72.9 ± 0.45
	1.5	365	62.9 ± 0.31
	2.0	473	74.2 ± 0.17
	2.5	365	63.6 ± 0.46
	3.0	473	73.8 ± 0.38
	3.5	365	64.3 ± 0.28
	4.0	473	73.6 ± 0.25
	4.5	365	63.7 ± 0.2
	5.0	473	73.3 ± 0.37

Kelvin probe force microscopy

Calculating the WF of the AFM-tip based on HOPG. The work function value of HOPG was 4.27 eV; The average potential value of the HOPG probe was measured to be 0.18 V.

$$\boldsymbol{\Phi}_{Sample} = \boldsymbol{\Phi}_{HOPG} - eV_{CPD} \qquad (S3)$$

$$V_{CPD} = V_{Sample} - V_{HOPG} \qquad (S4)$$

On the basis of the equations S3 and S4, the Φ_{sample} is calculated:

$$\boldsymbol{\Phi}_{Sample} = \boldsymbol{\Phi}_{HOPG} - e\left(V_{Sample} - V_{HOPG}\right) \qquad (S5)$$

Φ_{HOPG} = 4.27 V, V_{HOPG} = 0.18 V, thus the Φ_{sample} is determined:

$$\boldsymbol{\Phi}_{Sample} = 4.45 - eV_{Sample} \qquad (S6)$$

Table S4 Calculation of WF of the sample.

Sample		**λ / nm**	**Φ / eV**
MXene	0	—	3.67 ± 0.003
	0.5	365	3.66 ± 0.0033
	1.0	473	3.67 ± 0.0027
AZ^{+}-$Ti_3C_2T_x$	0	—	3.86 ± 0.0024
	0.5	365	3.80 ± 0.0025
	1.0	473	3.87 ± 0.0028
	1.5	365	3.79 ± 0.0026
	2.0	473	3.87 ± 0.0028
	2.5	365	3.79 ± 0.0032
	3.0	473	3.86 ± 0.0025
	3.5	365	3.79 ± 0.0027
	4.0	473	3.87 ± 0.0032
	4.5	365	3.79 ± 0.0027
	5.0	473	3.87 ± 0.0031

Table S5 Comparison the azobenzene molecular doping effect on the WF of different 2D materials.

Material	**Total WF shift (meV)**	**Ref.**
Au	40	[6]
MoS_2	30	[7]
Few-layer Graphene	~70	[8]
$Ti_3C_2T_x$ MXene	~70	This work

Conductance measurement

Table S6 Calculation of maximum photocurrent switching amplitude of the devices in five irradiation cycles.

Device / λ / nm	1	2	3	4
0	—	0.02 ± 1.0	0.05 ± 2.5	0.04 ± 3.0	0.07 ± 1.9
0.5	365	48.7 ± 1.7	47.3 ±1.9	49.2 ± 2.5	47.8 ± 3.5
1.0	473	0.22 ± 1.5	0.18 ± 2.9	0.2 ± 3.5	0.3 ± 2.5
1.5	365	47.7 ± 2.7	48.7 ± 3.3	48.1 ± 1.8	47.1 ± 2.4
2.0	473	0.1 ± 2.5	0.2 ± 3.1	0.7 ± 2.7	0.8 ± 1.3
2.5	365	49.7 ± 1.6	49.3 ± 2.6	46.8 ± 2.3	46.3 ± 1.9
3.0	473	0.3 ± 1.9	1.8 ± 2.5	1.9 ± 3.4	1.1 ± 2.9
3.5	365	50.0 ± 1.0	48.9 ± 3.2	47.2 ± 1.5	48.5 ± 2.7
4.0	473	2.1 ± 1.2	3.5 ± 2.9	2.7 ± 2.9	2.3 ± 3.2
4.5	365	50.8 ± 1.0	50.2 ± 2.0	48.3 ± 3.2	49.3 ± 3.0
5.0	473	3.7 ± 1.9	4.1 ± 2.8	3.6 ± 2.5	4.3 ± 2.1

Hall effect measurement

Table S7 Results of Hall effect measurement for the sample.

Sample	λ / nm	Mobility / $cm^2V^{-1}s^{-1}$	Carrier concentration / $*10^{14}$ cm^{-3}
AZ^+-$Ti_3C_2T_x$	—	0.71	1.22
	365	6.73	3.49
	475	0.76	1.50

References

1. Y. Q. Du, Z. K. Yan, W. B. You, Q. Q. Men, G. Y. Chen, X. W. Lv, Y. Y. Wu, K. C. Luo, B. Zhao, J. C. Zhang, R. C. Che, *Adv. Funct. Mater.*, 2023, **33**, 2301449.

2. B. Song, J. Zhao, B. Wang, R. Jiang, *Colloid. Surface. A*, 2009, **352**, 24–30.

3. M. Suda, N. Kameyama, A. Ikegami, Y. Einaga, *J. Am. Chem. Soc.*, 2008, **131**, 865–870.

4. R. Weber, B. Winter, I. V. Hertel, B. Stiller, S. Schrader, L. Brehmer, N. Koch, *Phys. Chem. B*, 2003, **107**, 7768–7775.

5. R. A. Shircliff, P. Stradins, H. Moutinho, J. Fennell, M. L. Ghirardi, S. W. Cowley, H. M. Branz, I. T. Martin, *Langmuir*, 2013, **29**, 4057−4067.

6. D. T. Nguyen, M. Freitag, C. Gutheil, K. Sotthewes, B. J. Tyler, M. Böckmann, M. Das, F. Schlüter, N. L. Doltsinis, H. F. Arlinghaus, B. J. Ravoo, F. Glorius, *Angew. Chem. Int. Ed.*, 2020, **59**, 13651–13656.

7. A. R. Brill, M. K. Kuntumalla, G. de Ruiter, E. Koren, *ACS Appl. Mater. Interfaces*, 2020, **12**, 33941–33949.

8. M. Döbbelin, A. Ciesielski, S. Haar, S. Osella, M. Bruna, A. Minoia, L. Grisanti, T. Mosciatti, F. Richard, E. A. Prasetyanto, L. De Cola, V. Palermo, R. Mazzaro, V. Morandi, R. Lazzaroni, A. C. Ferrari, D. Beljonne, P. Samorì, *Nat. Commun.*, 2016, **7**, 11090.